Science
AAAS

Tyrannosaur Life Tables: An Example of Nonavian Dinosaur Population Biology

Gregory M. Erickson, *et al.*

Science **313**, 213 (2006);
DOI: 10.1126/science.1125721

Science (print ISSN 0036-8075; online ISSN 1095-9203) is published weekly, except the last week in December, by the American Association for the Advancement of Science, 1200 New York Avenue NW, Washington, DC 20005.

from either equilibrium surface forces or hydrodynamic drainage. This is shown in Fig. 3A for the 10 mM SDS case at a series of times in the measurement conducted at a speed of 9.3 μm/s. The interdroplet separation in Fig. 3A flattens at the time closest to the largest repulsive force, marked t_2, 215.1 ms into a 430.2-ms measurement. The total pressure in Fig. 3B is a combination of the component contributions shown in Fig. 3, C and D. The strong positive pressure in Fig. 3B at time t_2 corresponds to the flat region in the interface profile in Fig. 3A.

The closest approach for the entire dynamic interaction event occurs in the retraction as shown at time t_3, 223.7 ms. The total radial pressure profile exhibits more features than any other curve in the time sequence in Fig. 3B, with a reversal from positive pressure at small radii to negative pressure at larger radii. This is due to the combination of pressure with different length scales from a positive equilibrium surface force at these interfacial separations and the negative hydrodynamic drainage pressure, as shown in Fig. 3, C and D. In contrast to the case involving only equilibrium interactions, for the dynamic interaction situation the closest approach, and hence opportunity for droplet coalescence to occur, can take place as the droplets move apart.

Ultimately it is clear that at velocities similar to those experienced through the Brownian motion of these droplets in solution, the contributions from hydrodynamic and surface forces are strongly coupled, and the relative length scales of these forces will influence which component dominates the interaction. The absence of a dimple in the interfacial profile when compared to drainage studies for larger droplets (*12*, *14*, *20*, *23*, *24*) is a product of both smaller droplet size and low deformation. The control of the velocity and interfacial tension in the experiment allows one to vary the relative effects so as to probe the situation where either surface force or hydrodynamic drainage can dominate the interactions behavior. For example, at even higher velocities, about twice those of the Brownian motion, the interfacial profile looks similar, but the contribution to the total pressure is then dominated by hydrodynamic drainage.

The thinning of the film in the radial center between the droplets at higher forces creates a remarkable coupling of the motion of the two droplets, which enhances the development of the smoothly varying minimum in the retract curve. The droplet velocity as a function of time at the axial and the edge positions of the droplet on the cantilever, for the 10 mM SDS concentration at 28 μm/s, is shown in fig. S2. As the two droplets approach, the displacement of the center of the interface slows as the film thins, and the two interfaces become stationary for small radial distances near the turnaround point. The axial center of the top droplet continues to lag behind the motion of the rest of the droplet, even at the beginning of the retract motion. The axial center of the top droplet then decouples its motion from the other droplet and accelerates to a velocity faster than the piezo drive with a recoiling motion before returning to rest. This behavior is described in the validated model without invoking interfacial rheological effects.

The agreement between the experimental data and the quantitative model identifies a number of important points related to describing interaction dynamics in liquid-liquid systems. This agreement is achieved by using the traditional no-slip boundary condition. This is contrary to what might be expected on the basis of some experimental observations of liquid drainage between rigid hydrophobic surfaces. One possible explanation is that the surface roughness of the oil-water interface is much smaller than that on a rigid surface, where deviations between theory and experiments have led to a heuristic correction to drainage models, referred to as a slip length. The quantitative visualization of the interfacial and pressure profiles provides a means of understanding the dynamic contributions from individual components in the physics of the interactions. The behavior of the droplet profile, pressure, and velocity upon the retraction presents an opportunity to probe systems possessing interfacial rheological characteristics and the impact of these on dynamic droplet-droplet interactions.

References and Notes

1. R. J. Hunter, *Foundations of Colloid Science* (Clarendon, Oxford, 1995).
2. J. N. Israelachvili, *Intermolecular and Surface Forces* (Academic Press, New York, 1992).
3. W. B. Russel, D. A. Saville, W. R. Schowalter, *Colloidal Dispersions* (Cambridge Univ. Press, New York, 1989).
4. H.-J. Butt, *J. Colloid Interface Sci.* **166**, 109 (1994).
5. W. A. Ducker, Z. G. Xu, J. N. Israelachvili, *Langmuir* **10**, 3279 (1994).
6. P. Mulvaney, J. M. Perera, S. Biggs, F. Grieser, G. W. Stevens, *J. Colloid Interface Sci.* **183**, 614 (1996).
7. D. E. Aston, J. C. Berg, *Ind. Eng. Chem. Res.* **41**, 389 (2002).
8. R. R. Dagastine, G. W. Stevens, D. Y. C. Chan, F. Grieser, *J. Colloid Interface Sci.* **273**, 339 (2004).
9. S. L. Carnie, D. Y. C. Chan, C. Lewis, R. Manica, R. R. Dagastine, *Langmuir* **21**, 2912 (2005).
10. S. L. Carnie, D. Y. C. Chan, R. Manica, *ANZIAM J.* **46(E)**, C808 (2005).
11. I. Ivanov, D. Dimitrov, *Surfact. Sci. Ser.* **29**, 379 (1988).
12. S. Abid, A. K. Chesters, *Int. J. Multiphase Flow* **20**, 613 (1994).
13. S. G. Yiantsios, R. H. Davis, *J. Fluid Mech.* **217**, 547 (1990).
14. A. K. Chesters, *Chem. Eng. Res. Des.* **69**, 259 (1991).
15. S. A. Nespolo, M. A. Bevan, D. Y. C. Chan, F. Grieser, G. W. Stevens, *Langmuir* **17**, 7210 (2001).
16. D. Bhatt, J. Newman, C. J. Radke, *Langmuir* **17**, 116 (2001).
17. D. Y. C. Chan, R. R. Dagastine, L. R. White, *J. Colloid Interface Sci.* **236**, 141 (2001).
18. R. R. Dagastine, T. T. Chau, D. Y. C. Chan, G. W. Stevens, F. Grieser, paper presented at the 7th World Congress of Chemical Engineering, Glasgow, Scotland, 10–14 July 2005.
19. J. C. Baygents, D. A. Saville, *J. Chem. Soc. Faraday Trans.* **87**, 1883 (1991).
20. E. Klaseboer, J. P. Chevaillier, C. Gourdon, O. Masbernat, *J. Colloid Interface Sci.* **229**, 274 (2000).
21. Materials and methods are available as supporting material on *Science* Online.
22. J. L. Hutter, J. Bechhoefer, *Rev. Sci. Instrum.* **64**, 1868 (1993).
23. J. N. Connor, R. G. Horn, *Faraday Discuss.* **123**, 193 (2003).
24. D. G. Goodall, M. L. Gee, G. Stevens, J. Perera, D. Beaglehole, *Colloids Surf. A* **143**, 41 (1998).

25. This work was supported by the Australian Research Council and by the National Science Foundation under Grant No. INT-020267.

Supporting Online Material

www.sciencemag.org/cgi/content/full/313/5784/210/DC1
Materials and Methods
Figs. S1 and S2

30 January 2006; accepted 1 June 2006
10.1126/science.1125527

Tyrannosaur Life Tables: An Example of Nonavian Dinosaur Population Biology

Gregory M. Erickson,[1]* Philip J. Currie,[2] Brian D. Inouye,[1] Alice A. Winn[1]

The size and age structures for four assemblages of North American tyrannosaurs—*Albertosaurus*, *Tyrannosaurus*, *Gorgosaurus*, and *Daspletosaurus*—reveal a pronounced, bootstrap-supported pattern of age-specific mortality characterized by relatively high juvenile survivorship and increased mortality at midlife and near the maximum life span. Such patterns are common today in wild populations of long-lived birds and mammals. Factors such as predation and entrance into the breeding population may have influenced tyrannosaur survivorship. This survivorship pattern can explain the rarity of juvenile specimens in museum collections.

Little is known about the population biology of nonavian dinosaurs. Did these animals show survivorship patterns akin to extant living dinosaurs—the birds, like the dinosaurs' cousins the crocodilians, or were they similar to more distantly related ecological analogs? Here, we use the age and size distribution from a death assemblage of the North American tyrannosaur *Albertosaurus sarcophagus* to produce an age-standardized ecological life table for a nonavian dinosaur population.

[1]Department of Biological Science, Florida State University, Tallahassee, FL 32306, USA. [2]Department of Biological Sciences, University of Alberta, Alberta T6G 2E, Canada.

*To whom correspondence should be addressed. E-mail: gerickson@bio.fsu.edu

We analyzed specimens from a monospecific assemblage found in 1910 by Brown (*1*) in sediments from the Horseshoe Canyon Formation along the Red Deer River, near Dry Island Buffalo Jump Provincial Park, Alberta, Canada. Renewed excavation of the site by the Royal Tyrrell Museum of Palaeontology, Drumheller, shows that 22 individuals are represented at the site (Table 1), making it the largest known aggregation of nonavian theropods from the Cretaceous Period and second only to the Cleveland Lloyd allosaur quarry (n = 40+) for a large species (*2*). Taphonomic analysis (*1*, *3*) reveals that the assemblage represents an attritional sampling (i.e., it is not representative of standing crop; fig. S2) from the local population (a group of coexisting individuals of the same species, whether a pack or individuals drawn from the area). The animals succumbed over a short period of time, perhaps through drought or starvation.

We selected fibulae and/or metatarsals from individuals representing 27% of the assemblage and used growth line counts to estimate ages at death (*3*–*6*). The smallest individual was included, as were some of the largest (Table 1). A regression of these data, along with age estimates for four other *A. sarcophagus* specimens from nearby sites within the formation (*7*) on femoral length, yielded $\text{Age}_{(\text{years})} = 0.033(\text{Femoral length}_{(\text{mm})}) - 9.765$, $r^2 = 0.919$ (fig. S1). The ages of the remaining individuals from the bone bed were estimated from this equation. Femoral lengths ranged from 0.32 to 1.16 m, and corresponding total lengths ranged from 2.2 to 10.1 m (table S1). Estimated ages for the dinosaurs spanned 2 to 28 years (Table 1). A life table (Table 1) (*3*, *8*) was constructed using these data, and a graph of age (x) versus survivorship (log l_x) was made (Fig. 1). We found a convex pattern of survivorship, with annual mortality ($q_{x(\text{year})}$) varying between 2 and 7% (mean = 3.7%) from ages 2 through 13, and between 10 and 33% (mean = 22.9%) from ages 14 through 23. (Note: 14 years is a plausible estimate for the typical age of sexual maturation in this taxon; see below.) Individuals surviving to 2 years of age had an average life expectancy of 16.60 years [6207 days divided by the 374 days in an early Maastrichtian year (*9*)]. A 90% confidence interval based on 10,000 bootstrap samples of these data supports the convex shape of the survivorship curve (Fig. 1 and fig. S4) (*3*).

Given that wild vertebrate populations, including carnivores, show high neonate mortality rates [e.g., a range of 50 to 80% per year is common in living crocodilians (*10*), birds (*11*), and mammals (*12*, *13*) despite major life history differences], this suggests similar rates in Dry Island *A. sarcophagus* and their complete survivorship curve resembling the sigmoidal type B_1 pattern (*14*) [a blend of Deevey type I and type III survivorship (*15*)] in which high neonate mortality gives way to high juvenile survivorship followed by increased rates of attrition later in development. Of the major survivorship patterns used to characterize populations for heuristic purposes (Fig. 2), types II and III can be ruled out as competing hypotheses in that they show linear and concave patterns, respectively. The remaining type I pattern is convex but is untenable because it occurs only in captive animals and humans from developed countries, where medical care and an absence of predation yield low neonate mortality.

The observed Dry Island *A. sarcophagus* survivorship pattern may be characteristic of tyrannosaurs as a whole, or it may reflect adaptation to local selective factors. Similar-sized single-population aggregations are not available for comparison. However, we surveyed a number of tyrannosaur fossils collected throughout specific North American formations (multipopulation sampling) and constructed composite life tables for these populations for comparison (tables S2 to S4) (*3*). Survivorship curves were constructed for *Tyrannosaurus rex* (n = 30) from the Hell Creek, Scollard, Willow Creek, and Frenchman formations; *Gorgosaurus libratus* (n = 39) from the Dinosaur Park and Two Medicine formations; and *Daspletosaurus* (n = 14) from the Dinosaur Park, Two Medicine, Oldman, and Lower Kirtland formations (*3*). As for the *A. sarcophagus* analysis, age was determined from growth line counts for 23% of the *T. rex* (n = 7), 13% of the *G. libratus* (n = 5), and 21% of the *Daspletosaurus* specimens (n = 3).

Like the Dry Island albertosaur population, survivorship in the outgroup tyrannosaurs—including *T. rex*, an animal with five times the body mass of *A. sarcophagus* (*7*)—was characterized by a convex pattern (Fig. 2). Post-neonate mortality rates averaging 2.5% (range 2.4 to 2.7%) were followed by increases in mortality averaging 20.9% (range 15.2 to 30.0%) before the demise of the cohorts. Maximum life span was 28 years for *T. rex*, 22 years for *G. libratus*, and 26 years for *Daspletosaurus*. Bootstrapped confidence in-

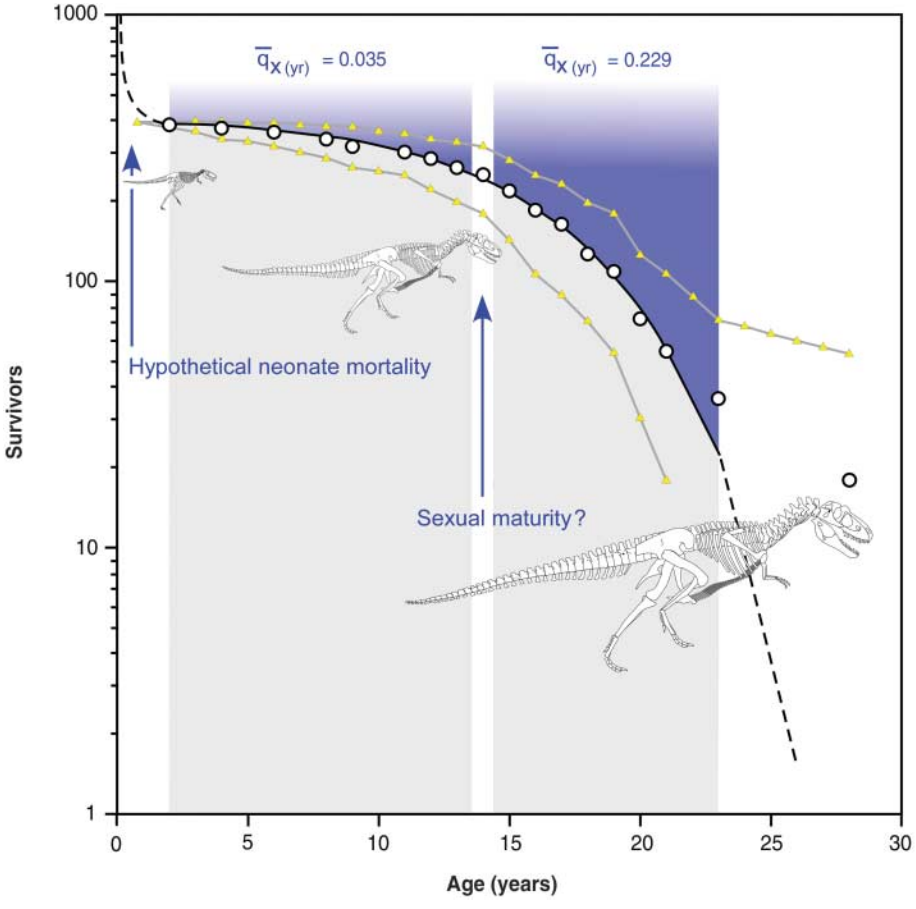

Fig. 1. Survivorship curve for a hypothetical cohort of 1000 *Albertosaurus sarcophagus* individuals, based on the Dry Island assemblage. Hypothesized neonate mortality is 60%. A period of relatively low mean mortality rates ($\overline{q}_{x(\text{year})}$) followed by a period of higher rates is indicated by the shaded regions. The progressive entrance of individuals into the breeding population may be reflected by the initial increases. A possible second increase in mortality late in development is denoted by dashed lines. Skeleton sizes during development at 2, 13, and 28 years are drawn in relative proportions to the maximal adult size of 10.1 m. The equation for the Gompertz curve is $n_x = n_0 \exp[(0.0073/0.1870)[1 - \exp(0.1870x)]]$, r^2 = 0.996, where n_x is the number of individuals alive at year x. Triangles show the 90% confidence interval based on 10,000 bootstrap samples of these data.

tervals supported the convex pattern in each taxon (fig. S4). Hence, it is unlikely that these samples could have come from populations with survivorship characteristics different from those of Dry Island *A. sarcophagus*, and this pattern appears to be characteristic of the entire group.

The ecological factors that contribute to the expression of type B_1 survivorship in extant vertebrate populations are well understood (*11*, *12*, *14*–*16*). High neonate mortality rates due to predation alone (disease, starvation, accidents, adverse climatic conditions, etc., also contribute) subside once a threshold size is reached. It appears that such a threshold was reached by age 2 in *A. sarcophagus*, when these animals had attained total lengths of 2 m, rivaling all other carnivorous theropods (deinonychosaurs, oviraptors, and ornithomimosaurs) in the Horseshoe Canyon Formation. It is here that *A. sarcophagus* survivorship diverged from patterns exhibited by their living archosaurian relatives, the crocodilians (Fig. 2), as well as other large ectothermal reptiles (*17*). Crocodilians, unlike nonavian dinosaurs such as tyrannosaurs (*6*, *7*), grow slowly, and their young remain susceptible to predation relatively late into development (*10*, *18*). Poor survivorship is further attenuated in crocodilians by rampant cannibalism that does not subside until they approach adult size (*10*). The relatively earlier decline in mortality and the evidence for gregariousness in tyrannosaurs (*1*, *19*), along with the rarity of postcranial bite marks from tyrannosaurs feeding on other tyrannosaurids (*20*), suggest that the rampant cannibalism seen in some theropods (*21*) was not a major factor in *A. sarcophagus* attrition. The *A. sarcophagus* survivorship pattern is also unlike that of most small birds, which do not show precipitous declines in mortality with attainment of adult size. This is because they remain highly susceptible to predation throughout life (*15*). In addition, adult size is often reached in a fraction of a year, so high neonate mortality rates contribute minimally to the first-year survivorship pattern (*11*, *15*). The hypothesized type B_1 survivorship pattern of tyrannosaurs is, however, similar to that seen in long-lived, typically large birds and mammals (*11*–*13*, *15*, *16*, *22*), which reach threshold sizes more rapidly than do ectothermal reptiles because of their relatively rapid growth rates (*23*), rates that are shared by tyrannosaurs (*7*).

The relatively low mortality rates among postneonate *A. sarcophagus* were maintained through about the 13th year of life, at which point they reached total lengths of ~6 m or 60% of their maximum recorded size (Fig. 1). A consequence of such low attrition is that ~70% of the animals surviving to 2 years of age were still alive at age 13. The taphonomic implications of this are intriguing. Neonate dinosaur remains are rarely recovered, either because they go unnoticed in the field or because their bones were consumed in their entirety or were completely broken down by the environment, hence they were unlikely to survive the vagaries of diagenesis to become fossilized (*12*, *13*, *15*). It seems unlikely that such considerations apply to the

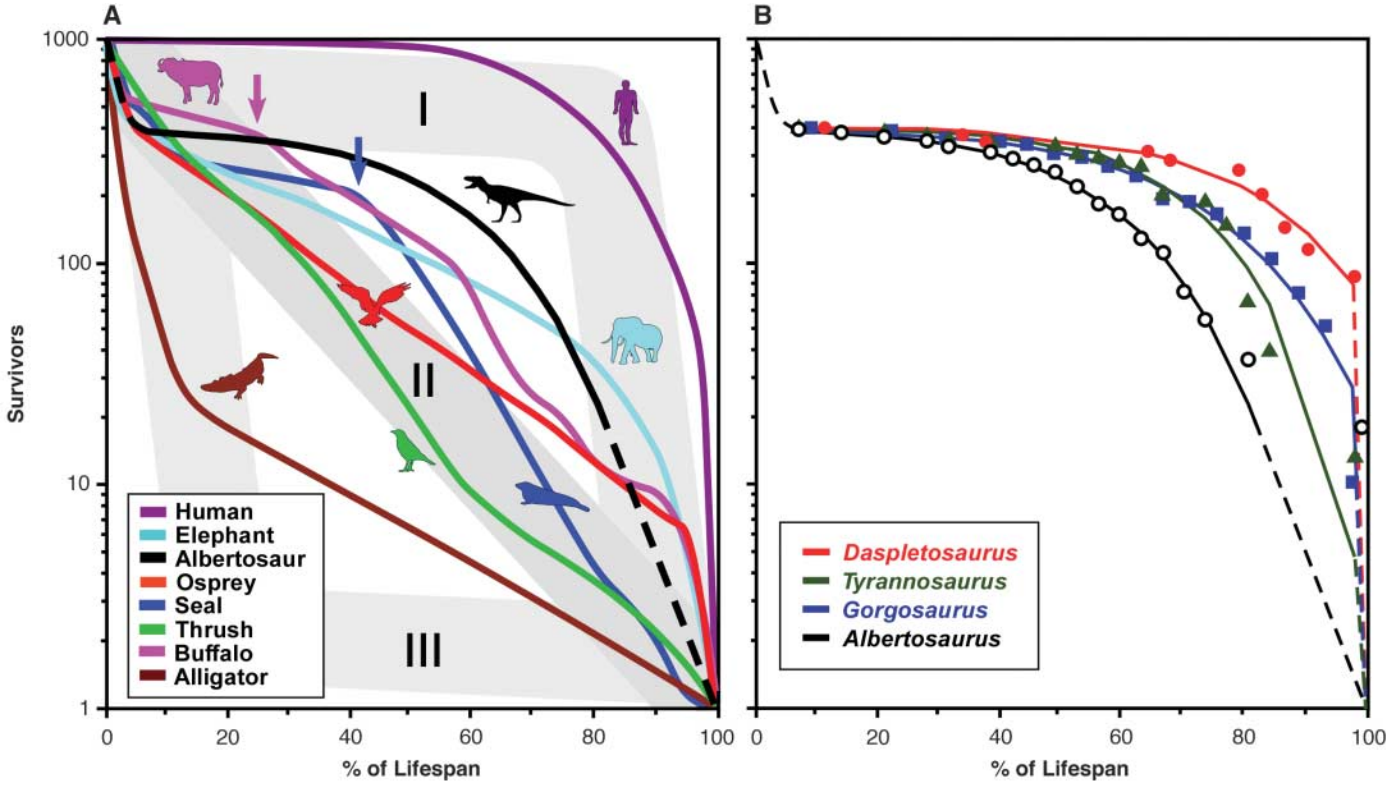

Fig. 2. *Albertosaurus* survivorship compared with patterns in living mammals, archosaurian relatives, and outgroup tyrannosaurs. The data are standardized according to ecological convention, with survivorship plotted on a logarithmic scale with respect to percent of maximum life span (*12*, *13*, *15*). (**A**) The shaded backgrounds show hypothetical ecological extremes used to characterize and contrast survivorship patterns (*15*). The convex type I pattern seen in some captive animals and in humans from developed countries (*8*, *15*) shows relatively low initial mortality followed by massive, senescence-driven die-offs as maximal life span is approached. The diagonal type II pattern [characteristic of small, short-lived birds, mammals, and lizards (*8*, *11*, *15*)] occurs in animals whose mortality is relatively constant throughout life. Populations showing the concave type III pattern [approached in crocodilians (*10*, *18*) and other large, long-lived reptiles (*17*)] experience high, early attrition; the few survivors that reach threshold sizes are likely to experience low mortality and to reach maximal life span. Long-lived, typically moderate to large birds (*22*) and mammals (*12*)—and presumably the tyrannosaur—show a sigmoidal type B_1 (*14*) pattern with high initial mortality rates, subsequent lower mortality, and increased mortality before extinction of the cohort. Note: Midlife, non–senescence-driven increases in mortality rates (arrows) often correspond to the onset of sexual maturity and breeding competition (*12*, *16*, *26*). (**B**) Survivorship in outgroup tyrannosaurs from multipopulation samples. All three outgroup species show bootstrap-supported (*3*) patterns of survivorship like that of the Dry Island *A. sarcophagus* population. Gompertz equation ($n_x = n_0 \exp[(a/g)[1 - \exp(gx)]]$) parameter values and fits: for *A. sarcophagus*, $a = 0.0073$, $g = 0.1870$, $r^2 = 0.9961$; for *Daspletosaurus* sp., $a = 0.0018$, $g = 0.2006$, $r^2 = 0.9669$; for *G. libratus*, $a = 0.0059$, $g = 0.2072$, $r^2 = 0.9944$; and for *T. rex*, $a = 0.002$, $g = 0.2214$, $r^2 = 0.9822$.

Table 1. Life table for Dry Island *A. sarcophagus*. TMP, Royal Tyrrell Museum of Palaeontology, Drumheller, Alberta, Canada; AMNH, American Museum of Natural History, New York City. Specimen numbers reflect elements definitively attributed to separate individuals from the assemblage. Mean length of life = 16.60 years. l_x values are the proportion of individuals alive at the beginning of each age class.

Specimen number	Age (years)	d_x (proportion dying)	l_x (proportion surviving)	q_x (interval mort. rate)	$q_{x(\text{year})}$ (annual mort. rate)†
TMP 2002.5.46*	2	0.0455	1.000	0.0455	0.0455
(Age not represented)	3	—	—	—	0.0241
TMP 2000.45.15	4	0.0455	0.9545	0.0477	0.0241
(Age not represented)	5	—	—	—	0.0254
TMP 1999.50.19	6	0.0455	0.9090	0.0501	0.0254
(Age not represented)	7	—	—	—	0.0267
AMNH 5229*	8	0.0455	0.8635	0.0527	0.0267
TMP 2000.45.7	9	0.0455	0.8180	0.0556	0.0556
(Age not represented)	10	—	—	—	0.0299
AMNH 5233*	11	0.0455	0.7725	0.0589	0.0299
TMP 1999.50.28	12	0.0455	0.7270	0.0626	0.0626
TMP 1999.50.26	13	0.0455	0.6815	0.0668	0.0668
TMP 2004.56.43, 2001.45.60	14	0.0909	0.6360	0.1429	0.1429
AMNH 5234,* AMNH 5218i	15	0.0909	0.5451	0.1668	0.1668
TMP 2001.45.49	16	0.0455	0.4542	0.1002	0.1002
AMNH 5235,* 5228	17	0.0909	0.4087	0.2224	0.2224
AMNH 5218ay	18	0.0455	0.3178	0.1432	0.1432
AMNH 5232,* 5231	19	0.0909	0.2723	0.3338	0.3338
AMNH 5218ac	20	0.0455	0.1814	0.2508	0.2508
TMP 1999.50.2	21	0.0455	0.1359	0.3348	0.3348
(Age not represented)	22	—	—	—	0.2952
TMP 2000.45.9	23	0.0455	0.0904	0.5033	0.2952
(Age not represented)	24 to 27	—	—	—	—
TMP 2004.56.48	28	0.0455	0.0449	1.000	1.000

*Specimens for which longevity was directly determined from growth line counts. †Values for the missing cohorts (ages 3, 5, 7, 10, 22) were calculated assuming constant annual mortality over the interval spanning missing ages (*3*).

relatively large juveniles and subadults of North American tyrannosaurs, and yet their remains (even partial remains) are rare (tables S2 to S4) (*24*, *25*). Some have speculated, on the basis of an implicit assumption of a constant rate of mortality, that tyrannosaurs must have rocketed to adult size in a few years or less (*25*), thereby leaving only a small fraction of development from which juveniles could have contributed to the fossil record. However, this notion is inconsistent with our growth curve (*7*). Instead, we suggest that these young animals simply had low mortality, just like older juveniles and subadults of most large terrestrial mammals today.

Midlife increases in mortality rate among extant vertebrates are not uncommon (*8*, *12*, *13*, *15*). Some of these increases reflect intermittent adverse environmental perturbation or human intervention. Those reflecting life history often coincide with the onset of sexual maturity and/or entrance into the breeding population, at which time the physiological demands of oviposition and fasting, increased injuries and stress from agonistic activity in competition for mates, and heightened exposure to predators take their toll. Notable examples of decreased survival associated with attainment of sexual maturity include some birds (*11*), large ungulates (*12*, *26*), and marine mammals (*16*). Given these considerations, it is plausible that the doubling of interval mortality rates and the quadrupling of annual mortality rates predicted between ages 11 and 15 reflect one or more of these same selective factors (Table 1). Horrific cranial bite scars attest that agonistic encounters with conspecifics were commonplace in tyrannosaurs (*19*). Schweitzer *et al*. (*27*) have found medullary bone deposits indicating sexual maturity in a young *T. rex*. The corresponding developmental stage in *A. sarcophagus* occurs at 14 to 16 years (fig. S3), approximately the age at which growth rates begin to slow in *A. sarcophagus* in association with somatic maturity (*7*). Slowing of somatic growth also signals the onset of sexual maturity in living reptiles (*28*).

If *A. sarcophagus* typically matured no later than 14 to 16 years of age, the survivorship curve indicates that ~25% of *A. sarcophagus* hatchlings reached reproductive maturity; the proportion that successfully reproduced is indeterminable. Among this group, few would have had long reproductive life spans because mortality rates escalated thereafter to greater than 23% per year.

In most long-lived vertebrates, mortality rates accelerate late in life. Such acceleration may reflect the debilitating effects of physiological senescence that promote greater susceptibility to disease, predation, and injury (*29*, *30*). Substantial declines in survival late in life are difficult to document because large sample sizes are required and few older individuals remain to be sampled. Although our samples contained only one or two large individuals, the largest and oldest known *T. rex*—the 28-year-old FMNH PR 2081—derives from a late (stationary) developmental stage (*7*) and shows numerous signs of senescence in the form of age-related disease (*31*). Similarly, the giant 10.1-m *A. sarcophagus* individual in our analysis is the largest (and presumably oldest) known for the taxon. It also was in the late stationary phase of development (*7*) and, like FMNH PR 2081, appears to be an outlier in the size distribution (fig. S2) and thus may have been of similar physiological condition at the time of its demise. As is true for the paucity of subadult specimens in museums, the estimated survivorship curve also provides a possible explanation for the rarity of such giants; just 2% of the population lived long enough to attain maximal size and age for the species.

References and Notes

1. P. J. Currie, *Gaia* **15**, 271 (1998).
2. J. H. Madsen Jr., *Bull. Utah Geol. Min. Surv.* **109**, 1 (1976).
3. See supporting material on *Science* Online.
4. P. M. Sander, *Ann. Sci. Natur. Zool. Paris* **13**, 213 (1990).
5. A. Chinsamy-Turan, *The Microstructure of Dinosaur Bone* (Johns Hopkins Univ. Press, Baltimore, MD, 2005).
6. G. M. Erickson, *Trends Ecol. Evol.* **20**, 677 (2005).
7. G. M. Erickson *et al.*, *Nature* **430**, 772 (2004).
8. T. A. Ebert, *Plant and Animal Populations: Methods in Demography* (Academic Press, San Diego, CA, 1999).
9. J. W. Wells, *Nature* **197**, 948 (1963).
10. G. Webb, C. Manolis, *Crocodiles of Australia* (Reed, French's Forest, New South Wales, Australia, 1989).
11. I. Newton, Ed., *Lifetime Reproduction in Birds* (Academic Press, London, 1989).
12. C. A. Spinage, *Ecology* **53**, 645 (1972).
13. B. Kurtén, *On the Evolution of Fossil Mammals* (Columbia Univ. Press, New York, 1988).
14. R. Pearl, J. R. Miner, *Q. Rev. Biol.* **10**, 60 (1935).
15. E. S. Deevey Jr., *Q. Rev. Biol.* **22**, 283 (1947).
16. J. R. Flowerdue, *Mammals: Their Reproductive Biology and Population Ecology* (Edward Arnold, London, 1987).
17. J. B. Iverson, *Can. J. Zool.* **69**, 385 (1991).
18. C. L. Abercrombie, K. G. Rice, C. A. Hope, in *Crocodilian Biology and Evolution*, G. C. Grigg, F. Seebacher, C. E. Franklin, Eds. (Surrey Beatty, Chipping Norton, New South Wales, Australia, 2000), pp. 409–418.
19. D. Tanke, P. J. Currie, *Gaia* **15**, 167 (1998).
20. A. R. Jacobsen, *Hist. Biol.* **13**, 17 (1998).
21. R. R. Rogers, D. W. Krause, K. C. Rogers, *Nature* **422**, 515 (2003).
22. S. Postupalsky, in *Lifetime Reproduction in Birds*, I. Newton, Ed. (Academic Press, London, 1989), pp. 297–313.
23. G. M. Erickson, K. Curry-Rogers, S. Yerby, *Nature* **412**, 429 (2001).
24. T. D. Carr, *J. Vertebr. Paleontol.* **19**, 497 (1999).
25. P. Larson, K. Donnan, *Rex Appeal* (Invisible Cities Press, Montpelier, VT, 2002).
26. R. D. Estes, *Behavioral Guide to African Mammals: Including Hoofed Mammals, Carnivores, Primates* (Univ. of California Press, Berkeley, CA, 1991).
27. M. H. Schweitzer, J. L. Wittmeyer, J. R. Horner, *Science* **308**, 1456 (2005).
28. R. M. Andrews, in *Biology of the Reptilia, Physiology D, Vol. 13*, C. Gans, F. H. Pough, Eds. (Academic Press, New York, 1982).
29. D. Promislow, *Evolution* **45**, 1869 (1991).
30. R. E. Ricklefs, A. Scheurlein, *Exp. Gerontol.* **36**, 845 (2001).

31. C. A. Brochu, *J. Vertebr. Paleontol. Mem.* **22**, 1 (2003).
32. We thank M. Norell and C. Mehling of the American Museum of Natural History and J. Gardner of the Royal Tyrrell Museum of Palaeontology for access to specimens in their care, and P. Larson and the Black Hills Institute of Geological Research Inc. for providing graphics for our use. Supported by NSF Division of Earth Sciences grant EAR 0207744 (G.M.E.).

Supporting Online Material
www.sciencemag.org/cgi/content/full/313/5784/213/DC1
Materials and Methods
Figs. S1 to S4
Tables S1 to S4
References

2 February 2006; accepted 1 June 2006
10.1126/science.1125721

Crystal Structure of Glycoprotein B from Herpes Simplex Virus 1

Ekaterina E. Heldwein,[1,2]* Huan Lou,[4] Florent C. Bender,[4] Gary H. Cohen,[4] Roselyn J. Eisenberg,[5] Stephen C. Harrison[1,2,3]

Glycoprotein B (gB) is the most conserved component of the complex cell-entry machinery of herpes viruses. A crystal structure of the gB ectodomain from herpes simplex virus type 1 reveals a multidomain trimer with unexpected homology to glycoprotein G from vesicular stomatitis virus (VSV G). An α-helical coiled-coil core relates gB to class I viral membrane fusion glycoproteins; two extended β hairpins with hydrophobic tips, homologous to fusion peptides in VSV G, relate gB to class II fusion proteins. Members of both classes accomplish fusion through a large-scale conformational change, triggered by a signal from a receptor-binding component. The domain connectivity within a gB monomer would permit such a rearrangement, including long-range translocations linked to viral and cellular membranes.

Herpes simplex virus type 1 (HSV-1) is the prototype of the diverse herpesvirus family, which includes such notable human pathogens as cytomegalovirus (CMV), Epstein-Barr virus (EBV), and Kaposi's sarcoma–associated herpesvirus (KSHV). Herpesviruses have an envelope, an outer lipid bilayer, bearing 12 surface glycoproteins. To deliver the capsid containing the double-stranded DNA genome into the host cell, HSV-1 must fuse its envelope with a cellular membrane. Among viral glycoproteins, only gC, gB, gD, gH, and gL participate in viral cell entry, and only the last four are required for fusion (*1*–*4*). All herpesviruses have gB, gH, and gL, which constitute the core fusion machinery (*5*). Of these, gB is the most highly conserved.

The virus attaches to a cell through a nonessential interaction of gC with heparan sulfate proteoglycan and through an essential interaction of gD with one of three cellular receptors: nectin-1, herpesvirus entry mediator (HVEM), or a specifically modified heparan sulfate (*6*). Crystal structures of the soluble ectodomain of gD, unbound and in complex with the ectodomain of HVEM (*7*, *8*), show that binding of gD and receptor causes the former to undergo a conformational change in which a C-terminal segment of the ectodomain polypeptide chain is released from a strong intramolecular contact. The liberated C-terminal segment may interact with gB or the gH/gL complex to trigger molecular rearrangements and, ultimately, fusion. The precise functions of gB and gH/gL are unknown. Both are required for entry, and either or both presumably receive the signal from gD and respond by undergoing a conformational change; gD itself is thought not to participate in the fusion process (*9*, *10*). Neither gB nor gH/gL has an obvious fusion peptide, but an indication that gB might be a fusion effector comes from the notable syncytial phenotype caused by certain mutations within the cytoplasmic domain of gB (*1*, *11*–*13*).

HSV-1 gB is a 904-residue protein. In the work reported here, we determined the crystal structure of a nearly full-length ectodomain of gB, residues Asp[103] to Ala[730] (*14*) (Fig. 1). Various features of the structure suggest that it is a fusion effector, an inference strengthened by its notable and unanticipated similarity to the structure of the fusion glycoprotein Gr of vesicular stomatitis virus (VSV), described in an accompanying paper (*15*). Domains that

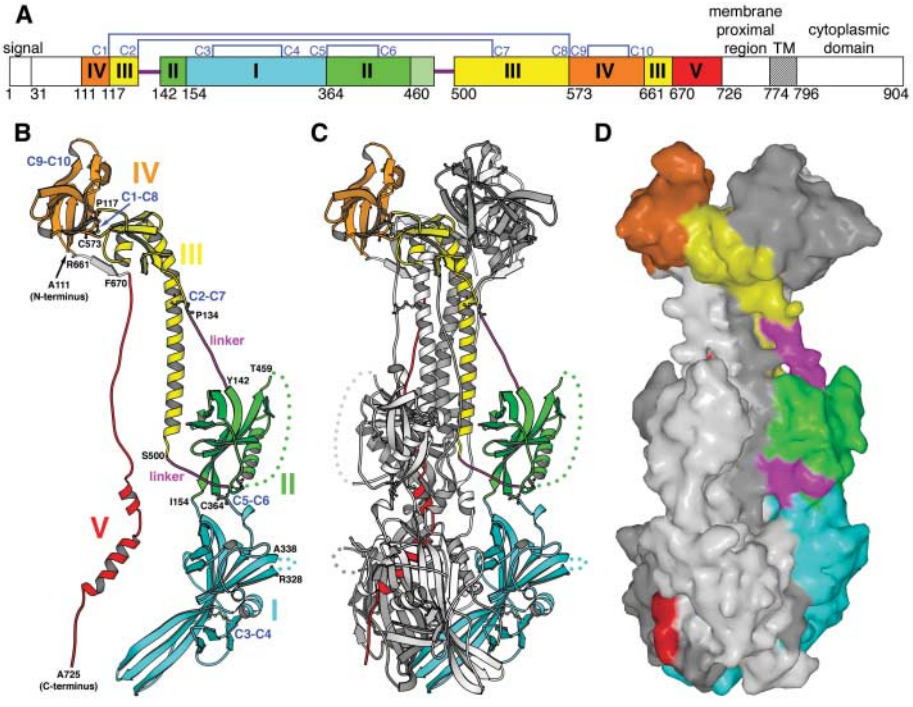

Fig. 1. (**A**) Domain architecture of gB. Domains observed in the crystal structure are highlighted in different colors, and their corresponding first residue positions are shown. (**B**) Ribbon diagram of a single gB protomer. The domains are rendered in colors corresponding to (A). Labeled residues (*26*) indicate the limits of individual domains and the disordered loop in domain I. Residues Arg[661] to Thr[669] of the shown protomer are in gray because they belong to domain III of a neighboring protomer. Residues Arg[661] to Thr[669] of the other neighboring protomer are included here and shown in yellow, because they contribute to a sheet in domain III of the shown protomer. Disordered segments are shown as dots of appropriate color. Disulfides are shown in ball-and-stick representation. Cysteines are numbered according to (A) and fig. S2. (**C**) gB trimer. Protomer A is the same as in (B). Protomer B is shown in white and protomer C in gray. (**D**) Accessible surface area representation of gB trimer. The coloring scheme is the same as in the rest of Fig. 1. Images were generated with the use of MOLSCRIPT (*27*) and SPOCK (*28*).

[1]Department of Biological Chemistry and Molecular Pharmacology, Harvard Medical School, [2]Laboratory of Molecular Medicine, [3]Howard Hughes Medical Institute, Children's Hospital, 320 Longwood Avenue, Boston, MA 02115, USA. [4]Department of Microbiology, School of Dental Medicine, [5]Department of Pathobiology, School of Veterinary Medicine, University of Pennsylvania, 240 South 40th Street, Philadelphia, PA 19104, USA.

*To whom correspondence should be addressed. E-mail: heldwein@crystal.harvard.edu